ACS APPLIED MATERIALS & INTERFACES

www.acsami.org

Research Article

Engineering Mesoporous Silica Nanoparticles for Targeted Alpha Therapy against Breast Cancer

Roger M. Pallares, Peter Agbo, Xin Liu, Dahlia D. An, Stacey S. Gauny, Steven E. Zeltmann, Andrew M. Minor, and Rebecca J. Abergel*

Cite This: *ACS Appl. Mater. Interfaces* 2020, 12, 40078−40084

Read Online

ACCESS | Metrics & More | Article Recommendations | Supporting Information

ABSTRACT: Targeted alpha therapy, where highly cytotoxic doses are delivered to tumor cells while sparing surrounding healthy tissue, has emerged as a promising treatment against cancer. Radionuclide conjugation with targeting vectors and dose confinement, however, are still limiting factors for the widespread application of this therapy. In the current study, we developed multifunctional silica nanoconstructs for targeted alpha therapy that show targeting capabilities against breast cancer cells, cytotoxic responses at therapeutic dosages, and enhanced clearance. The silica nanoparticles were conjugated to transferrin, which promoted particle accumulation in cancerous cells, and 3,4,3-LI(1,2-HOPO), a chelator with high selectivity and binding affinity for f-block elements. High cytotoxic effects were observed when the nanoparticles were loaded with ^{225}Ac, a clinically relevant radioisotope. Lastly, *in vivo* studies in mice showed that the administration of radionuclides with nanoparticles enhanced their excretion and minimized their deposition in bones. These results highlight the potential of multifunctional silica nanoparticles as delivery systems for targeted alpha therapy and offer insight into design rules for the development of new nanotherapeutic agents.

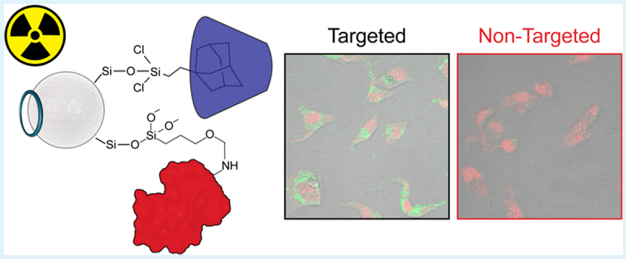

KEYWORDS: *silica nanoparticles, targeted alpha therapy, drug delivery, transferrin, actinium*

1. INTRODUCTION

The use of alpha radiation in targeted radiotherapy for cancer has great potential, as it enables the delivery of highly cytotoxic loads to targeted cells but minimizes damage to surrounding healthy tissue because of the short-range and high linear energy transfer of α particles.[1,2] It also overcomes several barriers to traditional radiation therapy, such as adaptive resistance and cell cycle progression.[1,2] As a result, several radionuclides, including ^{211}At, ^{213}Bi, and ^{212}Pb, which emit single α particles, are being clinically investigated as candidates for targeted alpha therapy.[3] In recent years, isotopes that emit multiple α particles in their decay chains, such as ^{225}Ac, have also received increased interest because they can act as *in vivo* α generators, enhancing the delivered dose.[4−6] Targeted alpha therapy relies on constructs formed by a chelating agent that complexes an α emitter and cancer-targeting vectors, such as antibodies or cell surface receptor binding peptides.[7] Some examples of promising α-generator immunoconjugates are the lintuzumab conjugate ^{225}Ac-HuM195 for myeloid leukemia treatment[5] and ^{227}Th-DOTA-trastuzumab for treating HER-2 positive breast and ovarian cancer.[8] Although initial preclinical and clinical studies have demonstrated the therapeutic potential of these targeting constructs, their formation kinetics and stability as metal complexes arose as major challenges.[3] Furthermore, radionuclides do not necessarily remain bound to the parent agent because of coordination chemistry specificities and high recoil energies, resulting in possible migration and toxic dose delivery to nontarget tissue.[9]

Recent progress to overcome this issue has been made by exploiting nanoparticles,[10] which have high surface-to-volume ratios[11,12] and can be easily functionalized with multiple chelating and targeting molecules.[13−17] For instance, doping multilayered gold-coated lanthanide phosphate nanoparticles with ^{225}Ac enhanced the confinement of recoiling daughters.[18,19] Although this platform improved the site retention of α particles and offered versatility for multifunctionalization with targeting moieties, the nonspecificity of the doping process did not fully prevent redistribution of the radiation to other organs. We intend to overcome these challenges by combining new nanoscale platforms for targeted alpha therapy with the demonstrated selectivity and specificity of 3,4,3-LI(1,2-HOPO), a chelating agent that forms highly thermodynamically and kinetically stable chelates with actinides and lanthanides.[20,21] Because complexes formed by HOPO-based chelators and radionuclides show very poor cellular uptake and

Received: June 18, 2020
Accepted: August 10, 2020
Published: August 11, 2020

Scheme 1. Bioconjugation of Multifunctional Mesoporous Silica Nanoparticles[a]

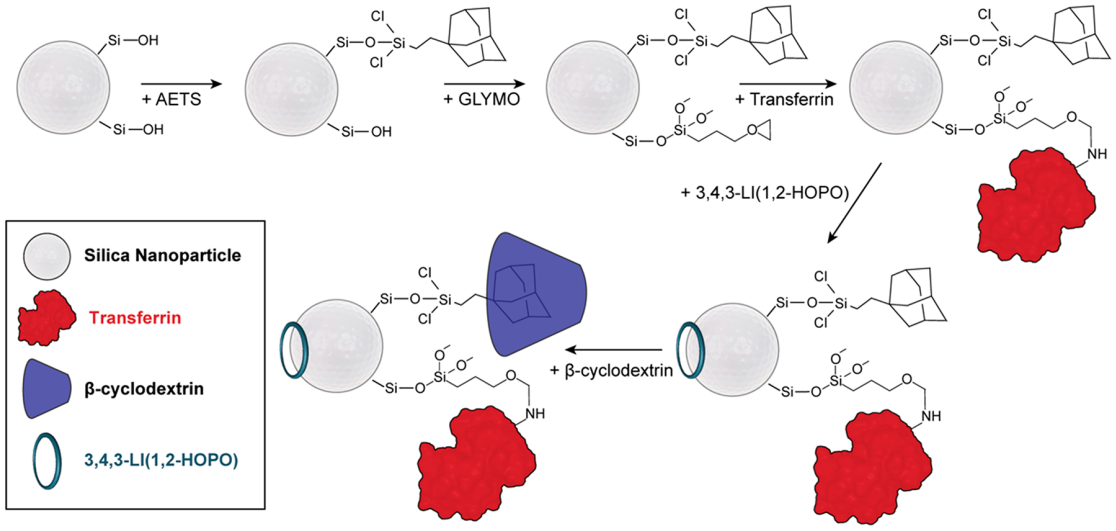

[a]The nanoparticles were conjugated with β-cyclodextrin using adamantylethyltrichlorosilane (AETS), transferrin using (3-glycidyloxypropyl)-trimethoxysilane (GLYMO), and 3,4,3-LI(1,2-HOPO).

lack therapeutic performance by themselves,[22,23] we used mesoporous silica nanoparticles (MSNPs) conjugated with targeting proteins as delivery vehicles, which are biocompatible and easy to functionalize,[24−27] and show high surface-to-volume ratios that improve the loading of therapeutic cargo.[28−30]

Here, we show that mesoporous silica nanoconstructs can be used as therapeutic agents for targeted alpha therapy. The MSNPs were functionalized with transferrin, which targeted breast cancer cells and promoted particle internalization, and 3,4,3-LI(1,2-HOPO) chelator. The nanoconstructs were biocompatible and only induced cytotoxic effects after functionalization with ^{225}Ac. *In vivo* studies showed that MSNPs improved the excretion of radionuclides, thus preventing their deposition into the bone matrix.

2. RESULTS AND DISCUSSION

2.1. Synthesis and Bioconjugation of Multifunctional Silica Nanoconstructs. Multifunctional MSNPs displaying cancer-targeting vectors, chelating molecules, and stabilizing agents were obtained using a multistep functionalization protocol (Scheme 1). We selected 140 nm spherical MSNPs (Figure 1a,b) as nanoconstruct cores because they are widely used as delivery vehicles in nanomedicine.[31,32] The synthesized nanoparticles had a hierarchical structure (Figure S1, Supporting Information) with pore diameters of 3.2 ± 0.6 nm and a characteristic X-ray diffraction peak (2θ) at 23° (Figure S2), which were consistent with previous literature results.[33−35] The MSNP surface was then sequentially modified with adamantanyl- and epoxy-containing molecules (Figure 1c), acting as anchoring points for stabilizing and targeting agents, respectively.

Since the transferrin receptor is upregulated on the surface of many cancer types, including breast cancer cells,[36] transferrin was used as a targeting vector with a density of 1739 ± 442 transferrins per MSNP (Figure S3). 3,4,3-LI(1,2-HOPO) was adsorbed on the nanoparticles by exploiting the strong adsorption capacity of MSNPs for nitrogen-rich aromatic compounds.[37,38] This chelator was chosen because

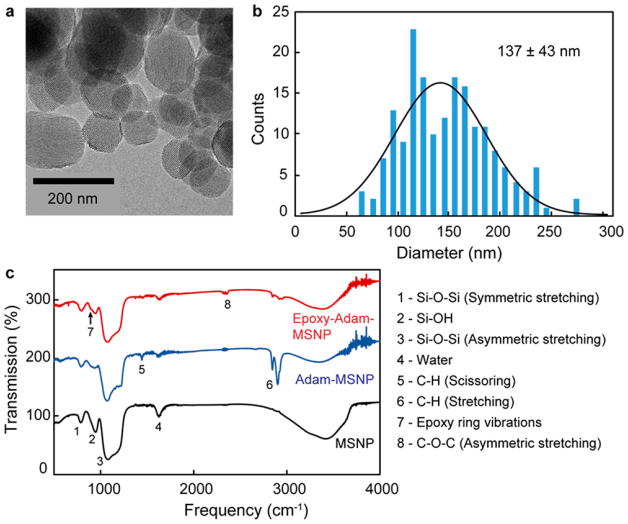

Figure 1. Characterization of mesoporous silica nanoparticles. (a) Representative transmission electron microscope (TEM) image and (b) size distribution of silica nanoparticles. The nanoparticle diameters were 137 ± 43 nm. (c) FTIR spectra of the particles before and after surface modifications with adamantanyl- (Adam) and epoxy-containing molecules. The spectra have been offset for clarity.

it shows high binding affinity and selectivity for f-block elements[20,21] and preserves its chelating performance when adsorbed on nanoparticle surfaces.[39] For stabilization, we selected β-cyclodextrin, which is commonly grafted on nanoparticle surfaces to improve colloidal biocompatibility, solubility, and stability.[40−42] After functionalization, the nanoparticles had an organic layer on the surface (Figure S4) characteristic of protein conjugation,[31] which was rich in nitrogen as observed by energy-dispersive X-ray spectroscopy (Figure S5). Moreover, the nanoparticle hydrodynamic diameter increased from 152 ± 10 to 173 ± 6 nm (Figure S6) after functionalization, and the resulting MSNPs had a zeta potential of −24.9 ± 1.8 mV (Figure S7), confirming their colloidal stability in solution.

https://dx.doi.org/10.1021/acsami.0c11051
ACS Appl. Mater. Interfaces 2020, 12, 40078−40084

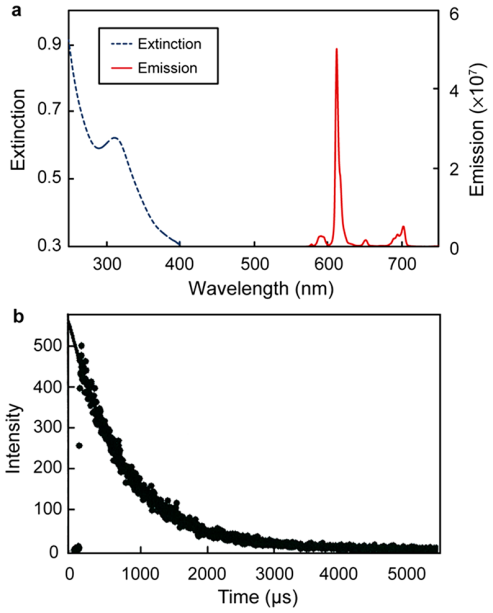

Figure 2. Spectroscopic characterization of Eu−HOPO−MSNPs. (a) Extinction and emission spectra and (b) time-resolved luminescence of Eu−HOPO−MSNPs (864 μg/mL) in 50 mM HEPES (pH 6.5). The excitation wavelength for luminescence experiments was 312 nm.

2.2. Characterization of Metal Complexation in Silica Nanoconstructs. To study metal complexation in nanoparticles, we used europium, which is frequently employed as a surrogate for trivalent actinides[43,44] because its ligand-sensitized luminescence provides information about metal coordination.[45] After conjugation with the metal, the multifunctional MSNPs showed extinction and emission peaks centered at 312 and 612 nm (Figure 2a), respectively, which are characteristic of Eu^{3+}−HOPO chelator complexes.[45,46] The extinction peak maximum was also consistent with the one recorded in the nanoparticle excitation spectrum (Figure S8). Moreover, the emission spectra of free Eu^{3+}−3,4,3-LI(1,2-HOPO) and Eu^{3+}−3,4,3-LI(1,2-HOPO)-containing multifunctional MSNPs (Eu−HOPO−MSNPs) were very similar (Figure S9), confirming that Eu^{3+} was complexed by the HOPO chelator on the particle surface. A loading of 214 ± 26 nM Eu^{3+}−3,4,3-LI(1,2-HOPO)/mg of MSNP was determined using the emission peak intensity at 612 nm of the nanoparticle solution (Figure S10). Time-resolved luminescence (Figure 2b) showed a single monoexponential decay lifetime (842 ± 84 μs) for Eu−HOPO−MSNPs, which was similar to the one previously reported for the free metal−ligand complex in solution (805 μs).[45] Moreover, when the empirical equations estimated by Kimura et al. were applied,[47] the number of inner sphere water molecules (q) for the Eu^{3+} complex on the nanoparticle surface was determined to be 0.8, which is consistent with the q values for other f-element−3,4,3-(1,2-HOPO) complexes in aqueous solution.[48,49] These results indicated that the adsorption of 3,4,3-LI(1,2-HOPO) in the multifunctional MSNPs did not significantly alter the coordination of the metal by this chelator.

2.3. Multifunctional Silica Nanoconstructs as Carriers for Radionuclides. After the synthesis and characterization of Eu−HOPO−MSNPs, we expanded our study using two α-generating radioisotopes. ^{225}Ac was chosen because it is clinically studied for targeted alpha therapy,[4−6] and ^{238}Pu was

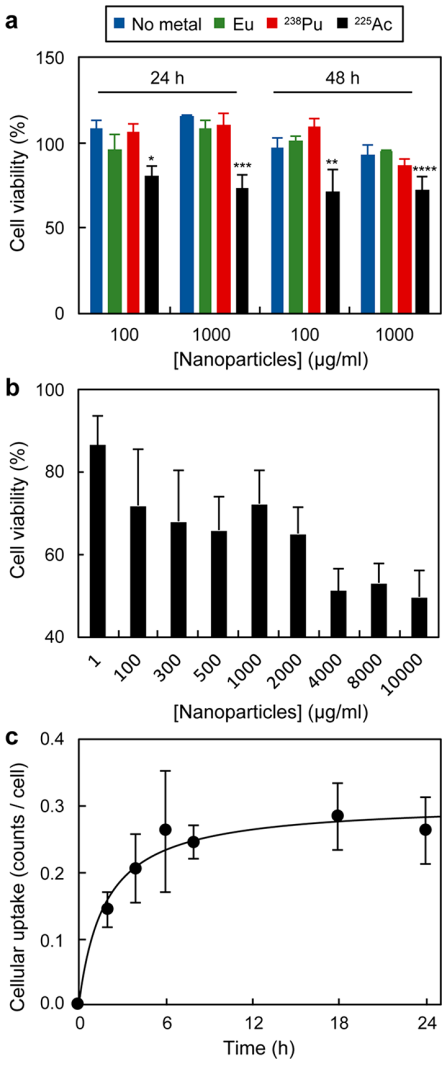

Figure 3. Therapeutic effect of multifunctional MSNPs. (a) Cell viability of BT-549 cells after 24 and 48 h of treatment with 100 or 1000 μg of MSNPs/mL. (b) Cell viability of BT-549 cells after 48 h of treatment with different concentrations of ^{225}Ac−HOPO−MSNPs. (c) Cellular uptake of ^{225}Ac−HOPO−MSNPs (200 μg/mL) as a function of time. (*), (**), (***), and (****) indicate the only groups that are significantly different from the control group with $p < 0.05$, $p < 0.01$, $p < 0.005$, and $p < 0.001$, respectively (one-way ANOVA with post hoc Tukey HSD test). All experiments were performed in triplicate; error bars represent 1 standard deviation of the measurements.

selected because it generates multiple α particles in its decay chain and shows higher availability and longer half-life (87.7 years[50]), which facilitate its handling. Although ^{238}Pu is not a front-runner isotope for therapeutic applications because it is a long-lived radionuclide that induces low radioactive dose, it allowed us to obtain fundamental information regarding nanoparticle biodistribution and excretion. The functionalization protocol was adjusted for the radionuclides, and the resulting nanoparticles showed an activity of 686 nCi/mg ^{225}Ac−HOPO−MSNP and 244 nCi/mg ^{238}Pu−HOPO−MSNP. Before their activities were quantified, the nanoparticles were incubated with fresh HEPES buffer (50 mM, pH 6.5) and washed five to ten times to remove any excess radionuclide. By measuring the activity of the supernatant after

https://dx.doi.org/10.1021/acsami.0c11051
ACS Appl. Mater. Interfaces 2020, 12, 40078−40084

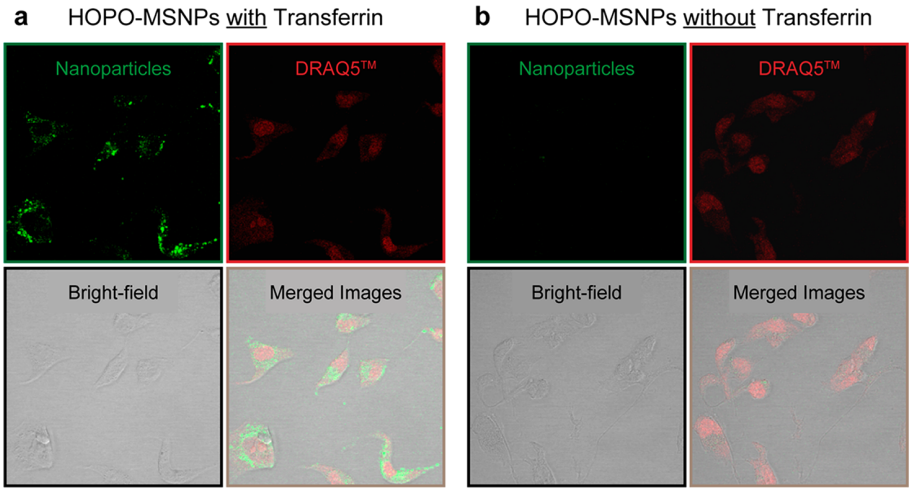

Figure 4. Confocal fluorescent images of BT-549 cells after incubation with multifunctional MSNPs (a) with or (b) without transferrin (200 μg/mL) for 48 h. The nanoparticles were labeled with fluorescein isothiocyanate and the cells were stained with DRAQ5.

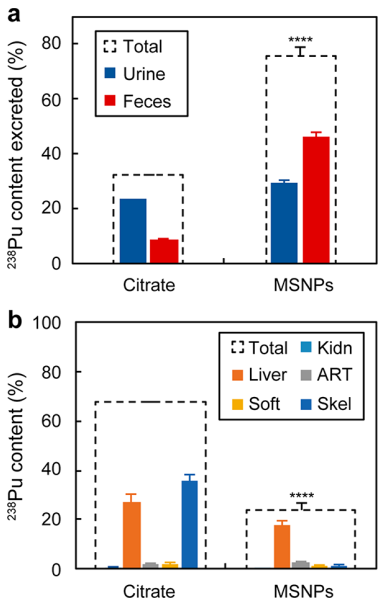

Figure 5. (a) Excretion and (b) biodistribution of ^{238}Pu delivered as multifunctional MSNP or citrate solutions at 48 h post injection. Soft, Kidn, ART, and Skel mean soft tissue, kidneys, abdominal remainder tissue, and skeleton, respectively. The animal models were young adult female Swiss Webster mice. The data is reported as a percentage of the recovered dose. The protocol followed in this study yields recoveries above 95% of the amount injected.[53] (****) indicates groups that are significantly different from the control (citrate) with $p < 0.001$ (two-sample t-test). All experiments were performed in quadruplicate; error bars represent 1 standard deviation of the measurements.

the washing steps, we guaranteed the metal complex was not released from the MSNP and it remained tightly attached. Finally, we quantified the activity of the washed particles, which confirmed the presence of the radionuclides on the MSNP surface.

2.4. Therapeutic Effect of Multifunctional Silica Nanoconstructs. Multifunctional MSNPs with and without f-block elements were incubated with breast cancer cells (BT-549) at two different particle concentrations of 100 and 1000 μg/mL. After 24 h, only the cells treated with ^{225}Ac-containing nanoparticles showed a decrease in cell viability (Figure 3a). Similar results were observed after 48 h at 100 μg of nanoparticles/mL, where only ^{225}Ac–HOPO–MSNP induced a cytotoxic effect. At 48 h and high particle concentration (1000 μg/mL), all cell viabilities decreased, but only those of cells treated with ^{225}Ac–HOPO–MSNPs were statistically significant. The stronger therapeutic effect of ^{225}Ac-containing nanoparticles was consistent with their higher activity load, faster decay of ^{225}Ac compared to ^{238}Pu, and production of faster decaying daughters, which all together results in a higher delivered dose to the cancer cells. Figure 3b shows that although the therapeutic effect of ^{225}Ac–HOPO–MSNPs was concentration-dependent (IC_{50} of 7.63 ± 2.14 mg/mL), similar responses were obtained using 100–2000 μg of nanoparticles/mL. Moreover, the similar cell viabilities observed between 24 and 48 h of treatments were consistent with cellular uptake, which peaked and stabilized at 6 h after particle addition (Figure 3c).

Next, the intracellular location and targeting performance of nanoparticles were investigated by confocal laser scanning microscopy. The cell nuclei were stained with DRAQ5 dye and multifunctional MSNPs without metal were labeled with fluorescein isothiocyanate to be visible in microscope images. The fluorescence signal from the multifunctional nanoparticles matched well with both DRAQ5 signal and cell profiles observed in the bright-field images (Figure 4a). Furthermore, z-stack of confocal microscopy images confirmed that the particles were internalized rather than deposited onto the cell surface (Figure S11). These results were consistent with a previous study that showed transferrin-functionalized nanoparticles being internalized by malignant cells into acidic intracellular compartments.[51] Confocal microscopy also demonstrated nanoconstruct targeting performance, where in the absence of transferrin, labeled MSNPs showed no internalization in BT-549 cells (Figure 4b). Taken together, these results confirmed that transferrin targets breast cancer cells and mediates nanoparticle internalization.

2.5. *In Vivo* Excretion and Biodistribution of Multifunctional Silica Nanoconstructs. Lastly, the excretion and internal accumulation of multifunctional MSNPs were investigated in a mouse model. Because these experiments

https://dx.doi.org/10.1021/acsami.0c11051
ACS Appl. Mater. Interfaces 2020, 12, 40078–40084

were designed to understand the biodistribution of silica nanoconstructs, we used the nanoparticles loaded with ^{238}Pu. Their low activity was enough to be used as a radiotracer, and they were easier to handle than their actinium counterparts. For the control group, Swiss Webster mice were treated with ^{238}Pu complexed with citrate, which is frequently used during the *in vivo* evaluation of decorporation treatments.[21,52] The metal-complexed nanoparticle or citrate solutions were injected intravenously, the mice were euthanized 48 h after injection, and excreta and tissues were radioanalyzed. All mice showed steady body weight during the study, and no dermal infections (visible and/or palpable), ascites, or impaired mobility were observed, suggesting a lack of acute toxicity. The multifunctional MSNPs significantly improved radionuclide excretion: 76.0 ± 3.1% of all ^{238}Pu was already excreted at 48 h postinjection when administered with nanoparticles, compared to only 32.3 ± 0.3% of ^{238}Pu when given as a citrate solution (Figure 5a). The primary route of MSNP excretion was through feces (46.5 ± 1.9% of total ^{238}Pu), which was consistent with previous MSNP data.[54]

The nanoparticles also minimized radionuclide deposition in the bone matrix (Figure 5b), which is the main accumulation area of f-block elements in the body.[55,56] While ^{238}Pu injected as a citrate solution primarily accumulated in the skeleton (35.6 ± 2.9% of total ^{238}Pu), almost no radioisotopes were detected in the bones of mice treated with the MSNPs (1.6 ± 0.4% of total ^{238}Pu). ^{238}Pu−HOPO−MSNPs that remained inside the mice after 48 h were mostly found in the liver (17.9 ± 2.1% of total ^{238}Pu), which likely reflects the excretion pathway of ^{238}Pu−HOPO−MSNPs since a previous report on MSNPs coated with similar stabilizing agents to the one used in this study showed 56.8% and 94.4% excretion after 48 and 96 h, respectively.[54] Hence, the administration of radioisotopes using nanoparticles greatly improved their excretion while minimizing internal deposition.

3. CONCLUSIONS

In summary, we demonstrated that MSNPs are effective delivery vehicles for targeted alpha therapy. The nanoparticles were functionalized with selective chelators for f-block elements and cancer-targeting vectors, which promoted particle uptake by breast cancer cells. While the nanoconstructs without metal or with Eu or ^{238}Pu were biocompatible at therapeutic dosages (between 100 and 1000 μg of nanoparticles/mL), loading with ^{225}Ac resulted in a cytotoxic response *in vitro*. Furthermore, *in vivo* studies with mice showed that the nanoconstructs improved the excretion of radionuclides, avoiding almost all internal deposition. All of these results indicate that mesoporous MSNPs, which improve the therapeutic response with minimal harmful side effects, are promising delivery systems for targeted alpha therapy.

■ ASSOCIATED CONTENT

Supporting Information

The Supporting Information is available free of charge at https://pubs.acs.org/doi/10.1021/acsami.0c11051.

Experimental section, quantification of transferrin on the nanoparticle surface, high-resolution TEM of MSNPs, X-ray diffraction spectrum of bare MSNPs, hydrodynamic and zeta potential of bare and functionalized nanoparticles, comparison between the Eu−HOPO complex and the Eu−HOPO−MSNP emissions, and z-stack of confocal microscope images of BT-549 cells after incubation with multifunctional MSNPs (PDF)

■ AUTHOR INFORMATION

Corresponding Author

Rebecca J. Abergel − *Chemical Sciences Division, Lawrence Berkeley National Laboratory, Berkeley, California 94720, United States; Department of Nuclear Engineering, University of California, Berkeley, California 94720, United States;* orcid.org/0000-0002-3906-8761; Email: abergel@berkeley.edu

Authors

Roger M. Pallares − *Chemical Sciences Division, Lawrence Berkeley National Laboratory, Berkeley, California 94720, United States;* orcid.org/0000-0001-7423-8706

Peter Agbo − *Chemical Sciences Division, Lawrence Berkeley National Laboratory, Berkeley, California 94720, United States;* orcid.org/0000-0003-3066-4791

Xin Liu − *Chemical Sciences Division, Lawrence Berkeley National Laboratory, Berkeley, California 94720, United States*

Dahlia D. An − *Chemical Sciences Division, Lawrence Berkeley National Laboratory, Berkeley, California 94720, United States;* orcid.org/0000-0002-8763-6735

Stacey S. Gauny − *Chemical Sciences Division, Lawrence Berkeley National Laboratory, Berkeley, California 94720, United States*

Steven E. Zeltmann − *National Center for Electron Microscopy, Molecular Foundry, Lawrence Berkeley National Laboratory, Berkeley, California 94720, United States; Department of Materials Science and Engineering, University of California, Berkeley, California 94720, United States*

Andrew M. Minor − *National Center for Electron Microscopy, Molecular Foundry, Lawrence Berkeley National Laboratory, Berkeley, California 94720, United States; Department of Materials Science and Engineering, University of California, Berkeley, California 94720, United States*

Complete contact information is available at: https://pubs.acs.org/10.1021/acsami.0c11051

Notes

The authors declare no competing financial interest.

■ ACKNOWLEDGMENTS

This work was supported by the Laboratory Directed Research and Development Program and by the Department of Energy (DOE), Office of Science, Office of Basic Energy Sciences, Chemical Sciences, Geosciences, and Biosciences Division, at Lawrence Berkeley National Laboratory, under Contract DE-AC02-05CH11231. S.E.Z. was supported by STROBE, a National Science Foundation Science & Technology Center under Grant No. DMR 1548924. The electron microscopy work was performed at the Molecular Foundry, a User Facility supported by the Office of Science, Office of Basic Energy Sciences, of the DOE under Contract DE-AC02-05CH11231. The authors thank Dr. Wayne W. Lukens for his help during the XRD measurements.

■ REFERENCES

(1) Kim, Y.-S.; Brechbiel, M. W. An overview of targeted alpha therapy. *Tumor Biol.* **2012**, *33* (3), 573−590.

(2) Mulford, D. A.; Scheinberg, D. A.; Jurcic, J. G. The Promise of Targeted α-Particle Therapy. *J. Nucl. Med.* **2005**, *46* (Suppl 1), 199S−204S.
(3) Elgqvist, J.; Frost, S.; Pouget, J.-P.; Albertsson, P. The Potential and Hurdles of Targeted Alpha Therapy − Clinical Trials and Beyond. *Front. Oncol.* **2014**, *3*, 324.
(4) McDevitt, M. R.; Ma, D.; Simon, J.; Frank, R. K.; Scheinberg, D. A. Design and synthesis of 225Ac radioimmunopharmaceuticals. *Appl. Radiat. Isot.* **2002**, *57* (6), 841−847.
(5) Jurcic, J. G.; Levy, M. Y.; Park, J. H.; Ravandi, F.; Perl, A. E.; Pagel, J. M.; Smith, B. D.; Estey, E. H.; Kantarjian, H.; Cicic, D.; Scheinberg, D. A. Phase I Trial of Targeted Alpha-Particle Therapy with Actinium-225 (225Ac)-Lintuzumab and Low-Dose Cytarabine (LDAC) in Patients Age 60 or Older with Untreated Acute Myeloid Leukemia (AML). *Blood* **2016**, *128* (22), 4050−4050.
(6) Miederer, M.; Scheinberg, D. A.; McDevitt, M. R. Realizing the potential of the Actinium-225 radionuclide generator in targeted alpha particle therapy applications. *Adv. Drug Delivery Rev.* **2008**, *60* (12), 1371−1382.
(7) Olafsen, T.; Elgqvist, J.; Wu, A. M. A. Protein Targeting Constructs in Alpha Therapy. *Curr. Radiopharm.* **2011**, *4* (3), 197−213.
(8) Heyerdahl, H.; Krogh, C.; Borrebæk, J.; Larsen, Å.; Dahle, J. Treatment of HER2-Expressing Breast Cancer and Ovarian Cancer Cells With Alpha Particle-Emitting 227Th-Trastuzumab. *Int. J. Radiat. Oncol., Biol., Phys.* **2011**, *79* (2), 563−570.
(9) De Kruijff, M. R.; Wolterbeek, T. H.; Denkova, G. A. A Critical Review of Alpha Radionuclide Therapy–How to Deal with Recoiling Daughters? *Pharmaceuticals* **2015**, *8* (2), 321−336.
(10) Pallares, R. M.; Abergel, R. J. Transforming lanthanide and actinide chemistry with nanoparticles. *Nanoscale* **2020**, *12* (3), 1339−1348.
(11) Pallares, R. M.; Su, X.; Lim, S. H.; Thanh, N. T. K. Fine-tuning of gold nanorod dimensions and plasmonic properties using the Hofmeister effects. *J. Mater. Chem. C* **2016**, *4* (1), 53−61.
(12) Pallares, R. M.; Wang, Y.; Lim, S. H.; Thanh, N. T. K.; Su, X. Growth of anisotropic gold nanoparticles in photoresponsive fluid for UV sensing and erythema prediction. *Nanomedicine (Lond.)* **2016**, *11* (21), 2845−2860.
(13) Dreaden, E. C.; Alkilany, A. M.; Huang, X.; Murphy, C. J.; El-Sayed, M. A. The golden age: gold nanoparticles for biomedicine. *Chem. Soc. Rev.* **2012**, *41* (7), 2740−2779.
(14) Pallares, R. M.; Thanh, N. T. K.; Su, X. Sensing of Circulating Cancer Biomarkers with Metal Nanoparticles. *Nanoscale* **2019**, *11*, 22152−22171.
(15) Qhobosheane, M.; Santra, S.; Zhang, P.; Tan, W. Biochemically functionalized silica nanoparticles. *Analyst* **2001**, *126* (8), 1274−1278.
(16) Yue, J.; Pallares, R. M.; Cole, L. E.; Coughlin, E. E.; Mirkin, C. A.; Lee, A.; Odom, T. W. Smaller CpG-Conjugated Gold Nanoconstructs Achieve Higher Targeting Specificity of Immune Activation. *ACS Appl. Mater. Interfaces* **2018**, *10* (26), 21920−21926.
(17) Pallares, R. M.; Choo, P.; Cole, L. E.; Mirkin, C. A.; Lee, A.; Odom, T. W. Manipulating Immune Activation of Macrophages by Tuning the Oligonucleotide Composition of Gold Nanoparticles. *Bioconjugate Chem.* **2019**, *30* (7), 2032−2037.
(18) McLaughlin, M. F.; Woodward, J.; Boll, R. A.; Wall, J. S.; Rondinone, A. J.; Kennel, S. J.; Mirzadeh, S.; Robertson, J. D. *PLoS One* **2013**, *8*, e54531.
(19) Symonds, P.; Jones, D. *Clin. Oncol.* **2013**, *25*, 567−568.
(20) Sturzbecher-Hoehne, M.; Deblonde, G. J. P.; Abergel, R. J. Solution Thermodynamic Evaluation of Hydroxypyridinonate Chelators 3,4,3-LI(1,2-HOPO) and 5-LIO(Me-3,2-HOPO) for UO2(VI) and Th(IV) Decorporation. *Radiochim. Acta* **2013**, *101*, 359−366.
(21) Sturzbecher-Hoehne, M.; Ng Pak Leung, C.; D'Aleo, A.; Kullgren, B.; Prigent, A. L.; Shuh, D. K.; Raymond, K. N.; Abergel, R. J. 3,4,3-LI(1,2-HOPO): In Vitro Formation of Highly Stable Lanthanide Complexes Translates into Efficacious In Vivo Europium Decorporation. *Dalton Trans.* **2011**, *40*, 8340−8346.
(22) Hagemann, U. B.; Mihaylova, D.; Uran, S. R.; Borrebaek, J.; Grant, D.; Bjerke, R. M.; Karlsson, J.; Cuthbertson, A. S. Targeted alpha therapy using a novel CD70 targeted thorium-227 conjugate in in vitro and in vivo models of renal cell carcinoma. *Oncotarget* **2017**, *8* (34), 56311.
(23) Hagemann, U. B.; Wickstroem, K.; Wang, E.; Shea, A. O.; Sponheim, K.; Karlsson, J.; Bjerke, R. M.; Ryan, O. B.; Cuthbertson, A. S. In Vitro and In Vivo Efficacy of a Novel CD33-Targeted Thorium-227 Conjugate for the Treatment of Acute Myeloid Leukemia. *Mol. Cancer Ther.* **2016**, *15* (10), 2422.
(24) Dang, Y.; Guan, J. Nanoparticle-based drug delivery systems for cancer therapy. *Smart Materials in Medicine* **2020**, *1*, 10−19.
(25) Zeng, X.; Liu, G.; Tao, W.; Ma, Y.; Zhang, X.; He, F.; Pan, J.; Mei, L.; Pan, G. A Drug-Self-Gated Mesoporous Antitumor Nanoplatform Based on pH-Sensitive Dynamic Covalent Bond. *Adv. Funct. Mater.* **2017**, *27* (11), 1605985.
(26) Li, C.; Wang, J.; Wang, Y.; Gao, H.; Wei, G.; Huang, Y.; Yu, H.; Gan, Y.; Wang, Y.; Mei, L.; Chen, H.; Hu, H.; Zhang, Z.; Jin, Y. Recent progress in drug delivery. *Acta Pharm. Sin. B* **2019**, *9* (6), 1145−1162.
(27) Cheng, W.; Nie, J.; Gao, N.; Liu, G.; Tao, W.; Xiao, X.; Jiang, L.; Liu, Z.; Zeng, X.; Mei, L. A Multifunctional Nanoplatform against Multidrug Resistant Cancer: Merging the Best of Targeted Chemo/Gene/Photothermal Therapy. *Adv. Funct. Mater.* **2017**, *27* (45), 1704135.
(28) Wang, Y.; Zhao, Q.; Han, N.; Bai, L.; Li, J.; Liu, J.; Che, E.; Hu, L.; Zhang, Q.; Jiang, T.; Wang, S. Mesoporous silica nanoparticles in drug delivery and biomedical applications. *Nanomedicine* **2015**, *11* (2), 313−327.
(29) Tang, F.; Li, L.; Chen, D. Mesoporous Silica Nanoparticles: Synthesis, Biocompatibility and Drug Delivery. *Adv. Mater. (Weinheim, Ger.)* **2012**, *24* (12), 1504−1534.
(30) Wu, M.; Meng, Q.; Chen, Y.; Du, Y.; Zhang, L.; Li, Y.; Zhang, L.; Shi, J. Large-Pore Ultrasmall Mesoporous Organosilica Nanoparticles: Micelle/Precursor Co-templating Assembly and Nuclear-Targeted Gene Delivery. *Adv. Mater. (Weinheim, Ger.)* **2015**, *27* (2), 215−222.
(31) Ferris, D. P.; Lu, J.; Gothard, C.; Yanes, R.; Thomas, C. R.; Olsen, J.-C.; Stoddart, J. F.; Tamanoi, F.; Zink, J. I. Synthesis of Biomolecule-Modified Mesoporous Silica Nanoparticles for Targeted Hydrophobic Drug Delivery to Cancer Cells. *Small* **2011**, *7* (13), 1816−1826.
(32) Moulari, B.; Pertuit, D.; Pellequer, Y.; Lamprecht, A. The targeting of surface modified silica nanoparticles to inflamed tissue in experimental colitis. *Biomaterials* **2008**, *29* (34), 4554−4560.
(33) Neimark, A. V.; Ravikovitch, P. I.; Grün, M.; Schüth, F.; Unger, K. K. Pore Size Analysis of MCM-41 Type Adsorbents by Means of Nitrogen and Argon Adsorption. *J. Colloid Interface Sci.* **1998**, *207* (1), 159−169.
(34) Kruk, M.; Jaroniec, M.; Sakamoto, Y.; Terasaki, O.; Ryoo, R.; Ko, C. H. Determination of Pore Size and Pore Wall Structure of MCM-41 by Using Nitrogen Adsorption, Transmission Electron Microscopy, and X-ray Diffraction. *J. Phys. Chem. B* **2000**, *104* (2), 292−301.
(35) Purnawira, B.; Purwaningsih, H.; Ervianto, Y.; Pratiwi, V. M.; Susanti, D.; Rochiem, R.; Purniawan, A. Synthesis and characterization of mesoporous silica nanoparticles (MSNp) MCM 41 from natural waste rice husk. *IOP Conf. Ser.: Mater. Sci. Eng.* **2019**, *541*, 012018.
(36) Daniels, T. R.; Bernabeu, E.; Rodríguez, J. A.; Patel, S.; Kozman, M.; Chiappetta, D. A.; Holler, E.; Ljubimova, J. Y.; Helguera, G.; Penichet, M. L. The transferrin receptor and the targeted delivery of therapeutic agents against cancer. *Biochim. Biophys. Acta, Gen. Subj.* **2012**, *1820* (3), 291−317.
(37) Chen, J.; Sheng, Y.; Song, Y.; Chang, M.; Zhang, X.; Cui, L.; Meng, D.; Zhu, H.; Shi, Z.; Zou, H. Multimorphology Mesoporous Silica Nanoparticles for Dye Adsorption and Multicolor Luminescence Applications. *ACS Sustainable Chem. Eng.* **2018**, *6* (3), 3533−3545.

https://dx.doi.org/10.1021/acsami.0c11051
ACS Appl. Mater. Interfaces 2020, 12, 40078−40084

(38) Dong, Y.; Lu, B.; Zang, S.; Zhao, J.; Wang, X.; Cai, Q. Removal of methylene blue from coloured effluents by adsorption onto SBA-15. *J. Chem. Technol. Biotechnol.* **2011**, *86* (4), 616−619.
(39) Pallares, R. M.; Carter, K. P.; Zeltmann, S. E.; Tratnjek, T.; Minor, A. M.; Abergel, R. J. Selective Lanthanide Sensing with Gold Nanoparticles and Hydroxypyridinone Chelators. *Inorg. Chem.* **2020**, *59* (3), 2030−2036.
(40) Zhu, J.; He, J.; Du, X.; Lu, R.; Huang, L.; Ge, X. A facile and flexible process of *β*-cyclodextrin grafted on Fe3O4 magnetic nanoparticles and host−guest inclusion studies. *Appl. Surf. Sci.* **2011**, *257* (21), 9056−9062.
(41) Banerjee, S. S.; Chen, D.-H. Magnetic Nanoparticles Grafted with Cyclodextrin for Hydrophobic Drug Delivery. *Chem. Mater.* **2007**, *19* (25), 6345−6349.
(42) Anirudhan, T. S.; Dilu, D.; Sandeep, S. Synthesis and characterisation of chitosan crosslinked-*β*-cyclodextrin grafted silylated magnetic nanoparticles for controlled release of Indomethacin. *J. Magn. Magn. Mater.* **2013**, *343*, 149−156.
(43) Heller, A.; Barkleit, A.; Bernhard, G. Chemical Speciation of Trivalent Actinides and Lanthanides in Biological Fluids: The Dominant in Vitro Binding Form of Curium(III) and Europium(III) in Human Urine. *Chem. Res. Toxicol.* **2011**, *24* (2), 193−203.
(44) Radchenko, V.; Mastren, T.; Meyer, C. A. L.; Ivanov, A. S.; Bryantsev, V. S.; Copping, R.; Denton, D.; Engle, J. W.; Griswold, J. R.; Murphy, K.; Wilson, J. J.; Owens, A.; Wyant, L.; Birnbaum, E. R.; Fitzsimmons, J.; Medvedev, D.; Cutler, C. S.; Mausner, L. F.; Nortier, M. F.; John, K. D.; Mirzadeh, S.; Fassbender, M. E. Radiometric evaluation of diglycolamide resins for the chromatographic separation of actinium from fission product lanthanides. *Talanta* **2017**, *175*, 318−324.
(45) Abergel, R. J.; D'Aléo, A.; Ng Pak Leung, C.; Shuh, D. K.; Raymond, K. N. Using the Antenna Effect as a Spectroscopic Tool: Photophysics and Solution Thermodynamics of the Model Luminescent Hydroxypyridonate Complex [EuIII(3,4,3-LI(1,2-HOPO))]−. *Inorg. Chem.* **2009**, *48* (23), 10868−10870.
(46) Pallares, R. M.; An, D. D.; Tewari, P.; Wang, E. T.; Abergel, R. J. Rapid Detection of Gadolinium-Based Contrast Agents in Urine with a Chelated Europium Luminescent Probe. *ACS Sensors* **2020**, *5* (5), 1281−1286.
(47) Zhang, P.; Kimura, T.; Yoshida, Z. Luminescence Study on the Inner-Sphere Hydration Number of Lanthanide(III) Ions in Neutral Organo-Phosphorus Complexes. *Solvent Extr. Ion Exch.* **2004**, *22* (6), 933−945.
(48) Sturzbecher-Hoehne, M.; Yang, P.; D'Aléo, A.; Abergel, R. J. Intramolecular sensitization of americium luminescence in solution: shining light on short-lived forbidden 5f transitions. *Dalton Trans.* **2016**, *45* (24), 9912−9919.
(49) Sturzbecher-Hoehne, M.; Kullgren, B.; Jarvis, E. E.; An, D. D.; Abergel, R. J. Highly Luminescent and Stable Hydroxypyridinonate Complexes: A Step Towards New Curium Decontamination Strategies. *Chem. - Eur. J.* **2014**, *20* (32), 9962−9968.
(50) Tchantchaleishvili, V.; Bush, B. S.; Swartz, M. F.; Day, S. W.; Massey, H. T. Plutonium-238: An Ideal Power Source for Intracorporeal Ventricular Assist Devices? *ASAIO J.* **2012**, *58* (6), 550.
(51) Wang, J.; Tian, S.; Petros, R. A.; Napier, M. E.; DeSimone, J. M. The Complex Role of Multivalency in Nanoparticles Targeting the Transferrin Receptor for Cancer Therapies. *J. Am. Chem. Soc.* **2010**, *132* (32), 11306−11313.
(52) Deblonde, G. J. P.; Lohrey, T. D.; An, D. D.; Abergel, R. J. Toxic heavy metal − Pb, Cd, Sn − complexation by the octadentate hydroxypyridinonate ligand archetype 3,4,3-LI(1,2-HOPO). *New J. Chem.* **2018**, *42* (10), 7649−7658.
(53) Durbin, P. W.; Kullgren, B.; Xu, J.; Raymond, K. N. Multidentate hydroxypyridonate ligands for Pu(IV) chelation in vivo: comparative efficacy and toxicity in mouse of ligands containing 1,2-HOPO or Me-3,2-HOPO. *Int. J. Radiat. Biol.* **2000**, *76*, 199−214.
(54) Lu, J.; Liong, M.; Li, Z.; Zink, J. I.; Tamanoi, F. Biocompatibility, Biodistribution, and Drug-Delivery Efficiency of Mesoporous Silica Nanoparticles for Cancer Therapy in Animals. *Small* **2010**, *6* (16), 1794−1805.
(55) Rees, J. A.; Deblonde, G. J. P.; An, D. D.; Ansoborlo, C.; Gauny, S. S.; Abergel, R. J. Evaluating the potential of chelation therapy to prevent and treat gadolinium deposition from MRI contrast agents. *Sci. Rep.* **2018**, *8* (1), 4419.
(56) An, D. D.; Kullgren, B.; Jarvis, E. E.; Abergel, R. J. From early prophylaxis to delayed treatment: Establishing the plutonium decorporation activity window of hydroxypyridinonate chelating agents. *Chem.-Biol. Interact.* **2017**, *267*, 80−88.

https://dx.doi.org/10.1021/acsami.0c11051
ACS Appl. Mater. Interfaces 2020, 12, 40078−40084